Long-Distance Electron Transport in Multicellular Freshwater Cable Bacteria

Tingting Yang[a#], Marko S. Chavez[a#], Christina M. Niman[a], Shuai Xu[a], Mohamed Y. El-Naggar[a,b,c,*]

[a] Department of Physics and Astronomy, University of Southern California, Los Angeles, CA 90089; [b] Molecular and Computational Biology Section, Department of Biological Sciences, University of Southern California, Los Angeles, CA 90089; [c] Department of Chemistry, University of Southern California, Los Angeles, CA 90089

*To whom correspondence should be addressed.
University of Southern California, 1002 Childs Way, MCB 220Q, Los Angeles, CA 90089-3502
(213) 740-2394; mnaggar@usc.edu

Abstract

Filamentous multicellular cable bacteria perform centimeter-scale electron transport in a process that couples oxidation of an electron donor (sulfide) in deeper sediment to the reduction of an electron acceptor (oxygen or nitrate) near the surface. While this electric metabolism is prevalent in both marine and freshwater sediments, detailed electronic measurements of the conductivity previously focused on the marine cable bacteria (*Candidatus* Electrothrix), rather than freshwater cable bacteria, which form a separate genus (*Candidatus* Electronema) and contribute essential geochemical roles in freshwater sediments. Here, we characterize the electron transport characteristics of *Ca.* Electronema cable bacteria from Southern California freshwater sediments. Current-voltage measurements of intact cable filaments bridging interdigitated electrodes confirmed their persistent conductivity under a controlled atmosphere and the variable sensitivity of this conduction to air exposure. Electrostatic and conductive atomic force microscopies mapped out the characteristics of the cell envelope's nanofiber network, implicating it as the conductive pathway in a manner consistent with previous findings in marine cable bacteria. Four-probe measurements of microelectrodes addressing intact cables demonstrated nanoampere currents up to 200 μm lengths at modest driving voltages, allowing us to quantify the nanofiber conductivity at 0.1 S/cm for freshwater cable bacteria filaments under our measurement conditions. Such a high conductivity can support the remarkable sulfide-to-oxygen electrical currents mediated by cable bacteria in sediments. These measurements expand the knowledgebase of long-distance electron transport to the freshwater niche while shedding light on underlying conductive network of cable bacteria.

Significance

Cable bacteria are multicellular filaments composed of up-to-thousands of end-to-end cells and are found worldwide in both marine and freshwater sediments. Remarkably, these cells gain energy from a long-distance electron transport process that carries electrons generated by sulfide oxidation in deeper sediment layers to drive oxygen reduction near the sediment-water interface. This electric metabolism requires an unusually high electronic conductivity, previously thought impossible in natural biological materials. However, the underlying mechanism(s) remain poorly understood, and previous characterization of the conductivity largely focused on marine cable bacteria. Here, we characterize and quantify the electronic conductivity of freshwater cable bacteria from sediments in Southern California, with emphasis on the role of the conductive periplasmic fiber network in routing electron transport along cables.

Introduction

Electron transfer reactions are fundamental to biological energy conversion. Respiratory organisms, for instance, gain energy by routing electron flow from an electron donor to a terminal electron acceptor through the network of reduction-oxidation (redox) cofactors that constitute the cellular electron transport chain (1). While the length scales of biological electron transfer events were long thought to be limited to nanometer distances and confined within individual cells, recent observations of fast long-distance extracellular and intercellular electron transport in microbial communities have upended this view (2). In fact, with the discovery of micron-scale electron transport via cytochrome nanowires from metal-reducing bacteria (3, 4), conductive bacterial biofilms (5, 6), inter-species electron

transfer in microbial consortia (7), and multicellular cable bacteria (8), the length scales of microbial electron transport observations have jumped from the nanometer to centimeter scale during the last 15 years.

The novel multicellular filamentous cable bacteria (CB), which belong to the *Desulfobulbaceae* family of Deltaproteobacteria (8), are a particularly interesting system for understanding the limits of biological electron transport given that they are the only known living structures capable of macroscopic (up to centimeter-scale) electron conduction. This macroscopic electron transport allows CB to gain energy from coupling sulfide oxidation by cells that dwell in the deeper sulfidic zone to oxygen reduction by cells near the surface sediment in both marine and freshwater sediments (8-11). The energy harnessed from this process allows CB to form a dense matrix (up to hundreds of meters per cm^2) that composes a majority of the biomass in sediment when blooming (12-16). While the molecular pathway of the conductive network responsible for centimeter-scale electron transport along the cables is not yet understood, the genomic basis and components allowing CB to carry out the two spatially-separated half-reactions are just beginning to come into focus. CB appear to oxidize sulfide by reversing the canonical sulfate reduction pathway, and are capable of sulfur disproportionation, while oxygen reduction is hypothesized to be driven by periplasmic cytochromes without energy conservation due to the absence of terminal oxidases (17, 18). The electrogenic sulfur oxidation and its coupling to distant redox events by CB significantly affects sulfur cycling and other essential geochemical processes, including nitrogen and metal cycling in global sediments (18, 19).

But what is the conductive pathway responsible for long-distance electron transport along an entire CB filament? The answer appears to lie in the unusual cell envelope of CB, where up-to-thousands of cells share a common outer membrane and parallel longitudinal ridges run along the surface of the entire filament (8, 20). These ridges reflect the presence of a network of long nanofibers (33 – 67 nm diameter) along the entire length of each cable in the periplasmic space between the common outer membrane and the cellular inner membranes (20, 21). Initial electrostatic force microscopy of these ridges showed striking electrostatic contrast (8), implicating the periplasmic nanofibers as the current carrying structures in marine CB filaments. More recently, the conductivity of intact air-dried marine CB filament and chemically extracted sheaths containing the nanofiber network was measured directly by various electronic techniques (22-24). Tens of nanoampere currents could be observed along both intact cable filaments and extracted nanofiber sheaths spanning hundreds of microns between microelectrodes in N_2/vacuum environments, but the conductance declined rapidly upon exposure to ambient air (22). Conductive atomic force microscopy (C-AFM) with stiff tips that scrape outer cell surface layers revealed that the conductive path indeed correlates with the network of individual periplasmic nanofibers (23). For the marine CB nanofibers, conductivities spanning the 10^{-2}-10^{1} S/cm range, with the upper end reaching as high as 79 S/cm, have been estimated (22); these values represent a record high for any biological structure. Furthermore, temperature-dependent electronic measurements suggest a thermally activated Arrhenius-type charge transport process with a low activation energy, suggesting that the CB conductive properties are comparable to organic semiconductor materials (24). The composition of the CB conductive nanofibers remains unknown, but recent evidence points

to yet-unknown core proteins rich in sulfur-ligated nickel cofactors that mediate electron transport through an enigmatic physical mechanism, and that the conductivity is diminished upon oxidation of the Ni/S groups (25).

On the basis of 16S rRNA gene sequencing, the CB clade consists of two novel candidate genera: the mostly marine *Candidatus* Electrothrix and mostly freshwater *Candidatus* Electronema (26). In addition, a more distant group of CB has been identified in ground water environments (17, 27). However, the abovementioned electronic characterization of CB conduction largely focused on marine CB, with the exception of two-probe measurements as part of a recent comparative study of diverse CB that included one freshwater CB enrichment culture (21). Freshwater sediments can contain CB populations at densities comparable to their marine counterparts, and their activity strongly influences the sediment geochemistry (11). Indeed, freshwater CB play an essential role in a cryptic sulfur cycle by stimulating sulfate reduction (28), and have been harnessed to significantly reduce methane emissions from rice-planted soil (29). From a materials perspective, investigations of freshwater CB may also uncover conductive biomaterials suited for applications in less saline environments that support higher electric fields than marine environments (28, 30). Here, we report on the recovery, phylogenetic analysis, imaging, and electronic characterization of *Ca.* Electronema CB from Southern California freshwater sediments using atomic force and multi-probe transport techniques.

Materials and Methods

Sediment sampling and incubation. Surface sediment and pond water was collected from two sampling sites. The first site, the Ballona Freshwater Marsh pond (33°58’15”N,

118°25’51”W), is a restored wetland that was previously filled and farmed for decades and is located 18 miles from downtown Los Angeles. The pond is seasonal (accessible ~ December to early June during the wet season). The second sampling site is Mungi Lake (34°6'6.192"N, 118°0'44.2224"W), located in the Los Angeles River Basin in the city of Arcadia, California. The sediment samples were collected from shallow water because the dissolved oxygen (DO) typically declines to zero during the summer months at depths greater than 5 meters (31). In the wintertime, less water stratification results in a higher DO concentration that can support cable bacteria growth in the lake bottom sediment. Mungi Lake samples were accessible year-round despite the lake shrinking during the dry season.

The top ~5 cm of sediment from both sites was sampled approximately every 3 months. Upon returning to the laboratory, the sediment was homogenized, sieved through a 5 mm-pore-size sieve, and carefully filled into glass jars, avoiding air bubbles in the sediment. The sediment jars were then incubated in a water bath at 15 °C, submerged in circulating, air-saturated water collected from the respective sites.

Cable bacteria filaments pickup. Filamentous bacteria were detectable after 2 weeks of incubation; occasionally, the filament density was high enough to be directly observed in sediment cracks (Figure 1). Over the incubation period, small sediment cores were taken from the sediment jars using plastic straws (8 mm diameter, 80 mm length) and transferred into small petri dishes filled with DI water. Long filaments were hand-picked under a dissection microscope using glass hooks made from capillary tubes, then washed successively at least three times in MilliQ water droplets. This extraction of cable bacteria was performed in a glove bag under an N_2 atmosphere.

16S rRNA gene sequence-based phylogenetic identification. Under a dissection microscope, three long filaments from each sampling site were washed and transferred into a sterile PCR-tube. Cells were lysed by freeze-thaw three times as described in a previous study (13). The lysates were directly used for PCR using the primer pair 8F and DSBB/1297R (32). PCR was performed according to manufacturer's instructions for the Q5® Hot Start High-Fidelity 2X Master Mix (New England Biolabs, USA). After 30 s at 98 °C for initial denaturation, PCR was performed with 35 cycles, consisting of 10 s at 98 °C, 30 s at 65 °C, and 45 s at 72 °C, followed by a final step of 2 min at 72 °C. The PCR amplicons were mixed and cloned using a Zero Blunt™ TOPO™ PCR Cloning Kit. Clones with a correct insertion were commercially sequenced (GENEWIZ, USA) using the vector primers M13F and M13R. Sequences were assembled in Sequencher 5.4, and their quality was checked manually. Alignment was performed in the ARB software package (arb-6.0.6) (33) using aligned sequences from SILVA database SSU 132 for reference (34), and manually refined subsequently. The 16S rRNA phylogenetic trees were generated by ARB. Trees that were built by the ARB neighbor joining algorithm and the maximum likelihood algorithm (RaxML) with a 50% positional conservation filter, with 1000 bootstrap replicates in all trees, were compared to make sure the trees had no conflicting branching. Representative sequences from this study were deposited in GenBank with accession numbers (OR244071 - OR244134).

Transmission electron microscopy (TEM). Bundles of filaments were washed thoroughly, deposited in small droplets of MilliQ water, and the CB filament-containing water droplets were then transferred and air-dried on PELCO® hexagonal Carbon-Formvar coated copper grids. The filament samples were unstained. High vacuum TEM was

performed by using an FEI Talos™ F200C (Thermo Fisher, USA) Electron Microscope at 80 kV, and the images were captured by a CCD camera.

Electrostatic Force Microscopy (EFM). EFM measurements were performed using an Oxford Instruments Asylum Research Cypher ES atomic force microscope (AFM). Substrates were affixed and electrically connected to sample discs. The CB were extracted from sediment using fine glass hooks, washed several times in DI water, and placed on the prepared substrates to dry. The sample discs were wired to the grounding pin of the AFM upon loading. Si probes with a Ti/Ir (5/20) coating, a nominal resonant frequency of 75 kHz (58-97 kHz range), a nominal spring constant of 2.8 N/m (1.4-5.8 N/m range), and a tip radius of 28±10 nm were used for all EFM measurements. High resolution EFM scans were performed following initial 'wide view' tapping AFM imaging to locate the CB filaments. For each EFM scan, a first pass scans the conductive probe in standard tapping without an applied tip bias, followed by a second 'nap' pass that retraces the first pass topography at a constant height above the sample. EFM was performed at different nap pass heights and tip voltage biases to arrive at optimal conditions and evaluate the voltage dependence. Electrostatic forces between the tip and sample shift the resonance frequency of the probe, resulting in a phase change of the cantilever, which was quantified for pixels representing specific features (e.g. nanofibers). The phase differences for each image (e.g. specific tip voltage bias) were averaged and their standard deviation taken.

Current-Voltage (I-V) measurements on Inter-Digitated Array (IDA) Microelectrodes. A 3 µm gap-size Au IDA (IDA Model#012129, ALS Co., Ltd, Japan) and a Pine® WaveDriver 200 Bipotentiostat/Galvanostat were used for electrical measurements. The IDA consists of two individually addressable arrays of interdigitated

gold microelectrodes (length, 2 mm; width, 3 µm; thickness: 100 nm). Copper wires were affixed to these two electrodes with silver paint (Product #: 16035, TED PELLA, Inc.) and covered with an epoxy layer at the contact points. The wires were then connected to the potentiostat, which swept the potential from -0.2 V to 0.2 V at a 10 µV/s sweep rate. All measurements were performed in an anaerobic chamber (95% N_2 and 5% H_2) (Bactron 300, Sheldon Manufacturing, Inc. Cornelius, OR). Control measurements prior to measurements of CB included open circuit (without water or cable bacteria), I-V measurements of an IDA on which a water droplet has been deposited (no cable bacteria), and I-V measurements made after the MilliQ water droplets were dried on the IDA (no cable bacteria). After these controls, CB filaments were washed and deposited in a small droplet of MilliQ water on the IDA surface. The CB filament-containing water droplet was then left to dry prior to the I-V measurement.

Conductive Atomic Force Microscopy. Conductive atomic force microscopy (C-AFM) was performed using an Oxford Instruments Asylum Research Cypher ES AFM. CB filaments were placed and dried across the insulating gaps between Au (Model#012129, 3 µm gap) or ITO (Model#012128, 5 µm gap) IDA microelectrodes from ALS Co., Ltd, Japan. For C-AFM current-mapping, ultra-sharp conductive single crystal diamond probes (AD-2.8-SS, Adama Innovations, Ltd), with < 5 nm tip radius, were used to image Mungi Lake CB in contact mode under N_2 perfusion. C-AFM current mapping was performed with a 0.1 Hz scan rate, 300 nN force, and a constant 5 V DC voltage bias applied between the probe and IDA. The probes and imaging parameters were selected to minimize disturbance to the sample while simultaneously eroding the insulating outer membrane enough to electrically probe the underlying periplasmic fibers. Prior to C-AFM, high

resolution tapping mode imaging was performed to spatially correlate the topography of the CB nanofibers to conductivity.

Point current-voltage (I-V) measurements were also performed to measure conduction along Ballona Marsh CB between the IDA microelectrodes and C-AFM tip (Si Probe ASYELEC.01-R2, Oxford Instruments, with a conductive Ti/Ir (5/20) coating and 28±10 nm tip radius) probing CB spots above the insulating quartz IDA gap under ambient conditions. At each point, the IDA voltage was swept for 5 consecutive cycles in the -10–10 V range with a 0.1 cycle/second scan rate, while the C-AFM probe was grounded and held in contact with the CB surface at a 450-510 nN force. All point-IV curves shown, including the insulating quartz background curve, are the average values taken from the 5 voltage cycles.

Four-probe Device Fabrication. Four-probe (4P) microelectrode devices were designed inhouse and fabricated by the University of California San Diego Nano3 cleanroom foundry service. Each device consisted of a series of parallel electrode bands. The bands were 3.5 mm long, 100 μm wide, and each one was connected on alternating sides to a 1.5 mm by 5 mm contact pad. The electrode band separation distances were variable, including multiple 20 μm and 200 μm gaps to assess different CB lengths. The fabrication process is briefly outlined as follows. 100 mm diameter and 0.5 mm thick SiO_2/Si wafers (Wafer model: 1583, University Wafer, Inc.) were used as substrates. Solvent cleaned wafers were coated with photoresist (PR) and a laser writer was used to project repeats of the device pattern onto the PR with UV light. E-beam evaporation was used to deposit a 5 nm Ti adhesion layer followed by a 100 nm Au layer onto the wafers. Solvents were used to

remove the excess Au/Ti layer and PR, leaving just the electrode patterns. As a final step, the wafers were coated in PR and each device was then diced into an 18 mm x 18 mm chip.

Four-probe Electrical Measurements. Four-probe (4P) measurements were made using an Agilent 4156C Precision Semiconductor Parameter Analyzer along with a Signatone 1160 series probe station. Thin copper wires (Product #: 1227, Train Control Systems) were electrically connected to the 4P contact pads with silver paint (Product #: 16035, TED PELLA, Inc.) and alligator clips attached to tungsten probes were used to connect the 4P device to the analyzer. Mungi Lake CB filaments were placed and dried across the electrodes of our devices. To deal with the high degree of variability between individual filaments, they were placed one at a time and I-V measurements performed after each deposition until current (from a conductive filament) was observed. To make the 4P measurement, a set of four electrodes on the device, with either a 20 μm or a 200 μm inner probe separation distance, were each wired to a source monitor unit within the analyzer. Current was swept between the outer two electrodes from -1 nA to 1 nA in step sizes of 100 pA. The voltage difference between the inner two electrodes (V_{inner}) was then recorded at each current step. Auto range voltage sensitivity with a voltage compliance of 5 V and an integration time of 1 PLC were used. A 2 second delay was used between each V_{inner} measurement to eliminate capacitive current contributions. Current sweeps were performed three times for the two inner probe gap sizes used. Average V_{inner} values for each current step were obtained from the three sweeps along with an error bar indicating the standard deviation. All 4P measurements were performed under an N_2 environment.

The single periplasmic fiber conductivity for the CB filaments measured at each inner electrode gap size was calculated from the formula $\sigma_{fiber} = \frac{L}{A\,N\,R_{cable}}$, where L is the

known spacing between the two inner electrodes, R_{cable} is the CB filament resistance, N is the average number of periplasmic fibers per cable bacteria filament, and A is the average cross-sectional area of a single periplasmic fiber. An average N = 35 fibers per CB was determined from TEM imaging. A was calculated from $\pi \left(\frac{d}{2}\right)^2$, with the periplasmic fibers assumed to be cylinders with average diameter d = 50 nm estimated from TEM imaging. R_{cable} was obtained as the inverse slope of best fit lines for the first CB current vs V_{inner} scan. Since current in each CB is carried by multiple periplasmic fibers, the $N\,R_{cable}$ factor, which represents the resistance of a single fiber, is based on a simplistic equivalent circuit model of a series of N identical parallel fiber resistors. Open circuit 2-probe controls (for each pair of electrodes on the 4P device) were performed prior to placing CB on the devices.

Results

1. Freshwater Cable Bacteria from Southern California Sediments

1.1 Identification of cable bacteria sampling sites. We identified two freshwater sediment sampling sites for recovery and subsequent measurements of cable bacteria (CB) in the Los Angeles area. The first site, Ballona Freshwater Marsh (Figure 1A), is a shallow seasonal freshwater pond which is heavily vegetated by aquatic plants that supply sufficient organic matter to the pond bottom sediment in the wet season (December to early June), and is dried out from approximately late June to December every year. The sediment profile from the site was brown-orange-colored at the surface and dark in color with a sulfide-smell below the surface, indicating a sharp oxic to sulfidic transition in the sediment. The second sampling site is Mungi Lake (Figure 1A), which is primarily fed by washes from

surrounding areas in Eastern Los Angeles and therefore is precipitation dependent. Mungi Lake has a much thinner and more densely packed sediment layer, compared to the Ballona Freshwater sediment, as the lake was converted from a gravel pit, with almost no aquatic plants and therefore no roots in the bottom surface sediment.

1.2 Southern California cable bacteria morphology: Thin silk-like filaments were directly observed by eye within cracks of sediment at both sampling sites. Following laboratory incubation in circulating water to enrich for CB (*Materials and Methods*), a high density of CB filaments was observed (Figure 1B). When observed with optical microscopy, the filament diameters varied from 0.7 µm to 3 µm, with thinner CB filaments usually observed within Mungi Lake sediments. Other than the diameter, there were no obvious morphological difference between the CB from the two sites. Occasionally, darker cells with slightly larger diameters than neighboring cells could be observed at seemingly random locations along the cable filaments (Figure 1C).

Transmission electron microscopy (TEM) imaging revealed that the freshwater CB display the characteristic previously observed parallel longitudinal periplasmic nanofibers that run along the along the entire CB filaments (Figure 2A). The estimated width of the fibers ranged from 49-57 nm, which is comparable to those of the marine cables (ca. 50 nm) (20). TEM imaging of CB recovered from the sediments occasionally revealed degraded cells along the filaments where only an ‘empty cage’ of the parallel nanofibers remained, appearing as darker material reflecting a higher electron-dense composition (Figure 2B) and likely corresponding to the enlarged cells in Figure 1. Imaging of the freshwater CB also revealed small intracellular electron-dense globules, consistent with polyphosphate

granules commonly observed in marine cables but not in freshwater CB previously (11, 18).

1.3 16S rRNA gene phylogeny of Southern California freshwater cable filaments and their associated bacteria. Three Ballona sediment CB filaments and three Mungi Lake sediment CB filaments were analyzed for 16S rRNA gene-based phylogenetic identification (Figure 3). All the Ballona sequences were within the family *Desulfobulbaceae*, and the majority (24/27 total Ballona sequences) grouped together with the freshwater CB sequence of *Ca.* Electronema palustris (96.7% - 97.3% similarity) (26). The three representative sequences slightly differ from each other indicating coexistence of different species in Ballona sediment. The few non-CB sequences all affiliated to sulfate-reducing bacteria from freshwater sediments (35, 36), with one sequence closely related to polycyclic aromatic hydrocarbon (PAH) degrading bacteria from a novel genus *Desulfoprunum benzoelyticum* (37).

The majority of Mungi Lake sequences affiliated within *Deltaproteobacteria* (26/35 clones). Three CB clones are closely related (> 99% similarity) to uncultured sequences (accession number FQ658891 and FQ658831) from a PAH-contaminated wetland collecting highway road runoffs (38). These Mungi Lake CB sequences share only 96.5% similarity to the *Ca.* Electronema nielsenii and are even further distantly related to the sequences of Ballona CB and *Ca.* Electronema palustris. Most of the non-CB Mungi Lake clones (18/26 clones) grouped together to sequences identified from an altiplanic cold lake in South America (39). Also in this group was a cluster (representative sequence: AJ389622, similarity 98.5%) resembling uncultured sulfate-reducers from a meromictic lake in Switzerland (40). Other Mungi Lake sequences affiliated to uncultured *Geobacter*

clones (EF192881) from a temperate artificial lake which receives mining wastes, and a polychlorinated-dioxin-dechlorinating community that can also perform oxidative degradation of the dechlorinated products, enriched from a polluted river sediment enrichment (41). Outside the *Deltaproteobacteria*, there were few sequences belonging to uncultured *Chlorobi* group (99.15% identity). One Mungi Lake clone was identified as *Ignavibacteria* (98.9% similarity to CP053446), which have been consistently found as the dominant flanking community in freshwater anammox bioreactors, presumably reducing nitrate to nitrite and degrading peptides, amino acids and EPS produced by anammox bacteria (42). One Mungi Lake clone shares 99.2% similarity to the uncultured sub group 1 of *Acidobacteria* from an Australian pasture soil (2-4 cm) (43); other Mungi Lake sequences include one that loosely related to a potential *Hydrogendentes* bacterium (44) and 4 clones that reside deep in the branch.

2. Electronic Characterization of Southern California freshwater cable bacteria

2.1 Electrostatic Force Microscopy. Electrostatic force microscopy (EFM) was used to visualize the electric field variations on Ballona CB filaments using a dual-pass measurement approach. Topographic (Figure 4A) and phase (Figure 4B) tapping mode images of CB were generated during the first pass, revealing in high resolution the surface ridge pattern along two consecutive CB cells. During the second pass, performed with a tip voltage bias at a set height (50 nm) above the retraced CB topography, the phase image (Figure 4C) captured the electric force gradient distribution as a result of the change in the resonant frequency of the probe arising from the CB-tip electrostatic interaction. Consistent with a previous report (8), the ridges and associated nanofibers exhibited conspicuously stronger electric forces relative to inter-ridge regions (Figure 4C), hinting at the unique

electronic properties of the underlying nanofibers. The voltage dependence of the CB-tip interaction was also investigated, revealing that the phase difference between the elevated ridges and inter-ridge regions is proportional to the tip voltage squared (Figure 4D).

2.2 Current-voltage measurements of freshwater cable bacteria across interdigitated array microelectrodes. For an initial assessment of freshwater CB conduction, current-voltage (I-V) measurements were performed along Ballona CB filaments bridging interdigitated array (IDA) microelectrodes in the oxygen-free environment of an anaerobic chamber (95% N_2, 5% H_2). In contrast to controls (open circuit IDA and deposited drops lacking CB), which showed no detectable current, multiple devices with deposited CB showed linear up-to-μA currents along intact filaments in response to voltage in the -0.2-0.2 V range (Figure 5).

In contrast to previous observations of marine CB, which exhibited a rapid and massive decline in conductance upon exposure to air (22), our observations of conductance in at least some freshwater CB filaments hinted at a higher degree of robustness upon oxygen exposure. For example, an IDA device with 2 CB filaments showed a modest slow increase in conductance during repeated I-V measurements over 3 hours in the oxygen-free atmosphere (Figure 5), ultimately reaching ± 3 μA in response to ± 0.2 V. Upon removal from the anaerobic chamber and exposure to air, the conductance immediately declined to 80% of the previous value, and slowly decayed until it ultimately stabilized at 63% of the oxygen-free value over 2.7 hours. When the IDA was moved back to the anaerobic chamber for further I-V measurements, the conductance again increased slowly until it stabilized after 2.4 hours (Figure 5). Interestingly, this behavior was filament-dependent; in another IDA that started with significantly smaller conductance under N_2 flow conditions (nA

current values for 0.8 V), exposure to ambient air caused immediate dramatic decline within minutes (Figure S1).

2.3 Conductive atomic force microscopy: point current-voltage spectra. The abovementioned conductance measurements probe transport longitudinally along multiple CB sections bridging IDA microelectrodes. We also performed point I-V conductance measurements through CB filaments between the underlying IDA and conductive AFM (C-AFM) tips; these measurements simultaneously probe longitudinal transport locally along specific CB sections and transversely across specific cells to the C-AFM tip above the filaments (Figure 6).

Tapping mode AFM images were first taken without voltage bias to visualize CB filaments laid on top of IDA microelectrodes and bridging 3-5 μm sections of the insulating quartz substrates (Figure 6A-C). No current response between the IDA and C-AFM tip was detected in response to applied voltage when the tip then probed the bare quartz surface near CBs. However, when the C-AFM tip probed points on the top surface of CB over quartz gaps, we detected currents up to tens of pA for voltages (-10-10 V) between the IDA and tip. These currents reflect a continuous path for electron transport from the underlying IDAs into cells, longitudinally along the conductive network of CB, and transversely into the overlying C-AFM tip. Interestingly, when such point I-V measurements were performed on CB exposed to air, the observed conductivity did not decay immediately, but slowly decreased over several hours, consistent with the IDA measurements reported above.

2.4 Conductive atomic force microscopy: mapping the conductive network of cable bacteria. In addition to the point I-V measurements described above, C-AFM was used in contact scanning mode to image the electron transport path along CB hanging off

microelectrodes under N_2 perfusion conditions (Figure 7). A constant voltage (5 V) was applied along the freshwater CB filaments between the microelectrode and an ultra-sharp (< 5 nm tip radius) conductive single crystal diamond C-AFM tip. Following a previous report on marine CB (23), a force set point was selected to gently scrape off the insulating outer membrane of the freshwater CB while allowing access to image the conductive network underneath. Figure 7 displays a current map, stitched together from 3 consecutive C-AFM images, of two CB filaments lying side-by-side and extending approximately 30 μm off a microelectrode. The imaging revealed parallel conductive paths consistent with the periplasmic nanofibers as the charge carriers in CB. Indeed, when compared with topographic imaging (Figure 7), the conductive paths coincided with the CB cell surface ridge pattern.

2.5 Four-probe transport measurements. To quantify the intrinsic conductivity of freshwater CB and their periplasmic nanofibers, we measured electronic transport along Mungi Lake CB deposited on custom fabricated four-probe (4P) microelectrode devices. In contrast to the two-probe IDA and C-AFM measurements described above, which include contributions from the CB-electrode contact resistances, the 4P measurements excluded contact resistance by routing current between two external microelectrodes and separately measuring the voltage drop across two inner microelectrodes. The resulting I-V plots (Figure 8) are shown for two separate inner probe separations, with the inverse slopes yielding whole CB resistances of 47 MΩ and 240 MΩ for the 20 μm and 200 μm lengths, respectively. By modeling the CB periplasmic nanofibers as current-carrying simple cylindrical wires forming a simplified circuit of parallel resistors, and taking into account

each nanofiber's estimated diameter (50 nm) and number of fibers per CB (~35), we arrive at a single nanofiber conductivity on the order of 0.1 S/cm, from both gap sizes.

Discussion

The appearance in many gene sequencing studies and increasing field observations suggest a cosmopolitan global distribution for cable bacteria (CB) in both marine and freshwater sediments (11, 45). Here, we identified two sampling sites (Figure 1) in the Los Angeles basin area, which served as a source for downstream phylogeny, microscopy, scanning probe, and electronic studies of freshwater CB. While CB have not been isolated into pure culture (46), the freshwater CB from both Ballona wetlands sediment and Mungi Lake sediment could be reliably enriched in laboratory incubations to provide a continuous supply for studies (Figure 1). Based on 16S rRNA gene sequence phylogeny (Figure 3), CB from the heavily vegetated Ballona sediments are closely related to *Ca*. Electronema palustris (26), which has been previously observed to associate with the roots of aquatic plants (47). On the other hand, CB from the non-vegetated Mungi Lake sediments are more closely related to those from PAH-contaminated sediment collecting water runoffs (38). The 16S rRNA gene analysis also revealed additional non-CB clones from both Ballona and Mungi Lake samples, many of which are highly similar to those from stratified and oligotrophic freshwater ecosystems (34). Although the relationship and functions of these bacteria are unclear, they likely represent cells firmly attached to CB filaments, as all the filaments were thoroughly washed before DNA extraction. The communities from both sites have representative lineages related to organic contaminant degradation, which corelate to the environmental background of the two sites. In Mungi Lake, for example,

various contaminants (chlordane, DDT, lead, dieldrin, polycyclic aromatic hydrocarbon, and polychlorinated biphenyls) have been identified previously (31).

Morphologically, our freshwater CB filaments exhibited the expected characteristics of previously studied CB (8, 20), including the cell surface ridge pattern and underlying periplasmic nanofiber network (Figures 2-4). The latter could be observed in transmission electron microscopy (TEM) of freshwater CB both within intact cells and, occasionally, as the remaining cage scaffold from naturally degraded cells (Figure 2). The typical single nanofiber width encountered in our freshwater CB was 53 ± 8 nm, which is consistent with the previously reported nanofiber thickness from marine CB (20) and recent characterization of a single strain freshwater CB enrichment culture (33 nm) (21). These results suggest that, while general morphological features are shared amongst diverse CB strains, the number and size of the ridges (and possibly their internal components) may depend on strain and environmental condition. However, similarly to previous measurements of marine CB (8), electrostatic force microscopy (EFM) captured stronger electric forces when scanning the cell surface above the ridges (Figure 4), again indicating the unique electric potential and charge distribution from the underlying conductive periplasmic nanofibers. By scanning the long-range electrostatic interaction between CB and tip at a fixed retrace height above the sample, we observed the expected voltage squared dependence of the EFM phase contrast (48), thereby unambiguously assigning EFM phase contrast to the electric force gradient rather than a topographic contribution. Conductive atomic force microscopy (C-AFM) with an ultra-sharp diamond tip that disrupts the insulating outer cell layer (Figure 7) offered an even more direct confirmation of the conductivity of underlying periplasmic nanofibers, by observing conductive paths

between the microelectrode and scanning tip that correlate with the CB ridge pattern. Furthermore, C-AFM point I-V spectra (Figure 6) confirmed a direct path for charge transport originating from the microelectrode below intact CB, along the internal periplasmic nanofiber, and into the C-AFM tip above the sample, consistent with the previously observed interconnectivity of the nanofiber network between cells (23). The latter measurements also illustrate a high degree of variability (Figure 6) in the conduction signal across different cables; it remains unclear whether this variability reflects heterogeneities intrinsic to different CB filaments or stems from culturing and/or sample preparation effects (including possible oxidative damage). Taken collectively, however, the EFM and C-AFM observations, performed here for the first time on freshwater CB, are consistent with previous analogous measurements on marine CB (8, 22, 23).

While their two-probe nature includes a contact resistance contribution, we found interdigitated array (IDA) microelectrodes to offer a convenient assessment of CB conduction properties (Figure 5) ahead of more sophisticated AFM and four-probe based techniques (Figures 6-8). The IDA platforms, which are commercially available, have been previously used to investigate conductivity in bacterial biofilms (5, 6), and result in high current signals (μA currents in Figure 5) as a result of assessing transport along multiple CB sections spanning the IDA inter-electrode gaps. Interestingly, these measurements hint that freshwater CB conductivity may have a somewhat higher degree of tolerance to oxygen exposure than previously reported for marine CB. Instead of an instantaneous and dramatic decline in conduction upon exposure to air (22), some of our freshwater CB samples exhibited a slow (hours) and only partial decline of the conduction upon exposure to air, which could be partially restored by re-insertion into an anaerobic chamber (Figure

5). While these observations showed a high degree of variability and therefore require a more detailed investigation, it is interesting to consider the possibility that the oxidative decline (or other damaging processes), thought to be a consequence of oxidation of Ni cofactors involved in electron transport (25), may not affect all sections of the cm long CB filaments simultaneously; under these conditions, IDA measurements, which probe multiple micrometer-scale electrode-crossing CB regions (e.g. 372 crossings in Figure 5 inset) may offer an advantage over techniques addressing entire CBs or specific CB regions. It is also interesting to consider an alternative possibility that the conductive properties of freshwater CB maybe intrinsically more oxygen-resistant than marine CB. In general, salt content affects the solubility of oxygen, which dissolves to 25% high levels in fresh water than saltwater. Indeed, previous CB studies verified 20% - 25% higher oxygen concentration at the surface of freshwater sediment (310 – 350 µM) (11, 28), compared to marine sediments (200 – 280 µM) (8-10, 13, 14, 49-52). Our results motivate a systematic investigation to correlate the oxygen availability in CB environments to both their conductivity and tolerance of electron transport to oxygen exposures.

When taking contact resistances of intact freshwater CB into account with four-probe measurements (Figure 8), we estimated the single nanofiber conductivity to be in the 10^{-1} S/cm range. This figure falls within the 10^{-2}-10^{1} S/cm range recently reported for marine CB (22, 24). While these measurements are performed under *ex situ* conditions, they motivate the question of whether the measured conductivities are sufficient to support the *in situ* activity of CB in sediments. From previous measurements of the CB filaments density in sediment incubations (~10^{8} - 10^{9} m^{-2}) and the electron current densities linking electrogenic sulfur oxidation to oxygen reduction (74 - 96 mA m^{-2}) (10, 13, 53, 54), one

arrives at a per cable current around 170 pA, which amounts to per nanofiber current of 5 pA given the average number of nanofibers seen in our cables. Assuming a driving voltage up to 1 V, representing the redox potential difference between the anodic sulfide oxidation and cathodic oxygen reduction half-reactions, for a typical nanofiber cross sectional area and length (e.g. several mm), these conditions requires a minimum nanofiber conductivity on the order of 0.1 S/cm. Remarkably, this heuristic calculation therefore sets a limit on conductivity that is consistent with the electronic measurements. It is also interesting to consider what the observed conductivities ((22-24) and this study) may teach us about the underlying physical electron transport mechanism in CB. It is common to interpret such extended transport in molecular systems in one of two limits: hopping between charge localizing sites such as redox factors (e.g. the hypothesized Ni/S groups of CB), or coherent band-like transport familiar from periodic systems including metals or semiconductors. In this context, the thermally activated nature of CB transport, and the estimate of the room temperature electron mobility at ~ 0.1 cm^2/Vs (24) are consistent with hopping transport, as the latter figure approaches but is still below the generally accepted minimum mobility ($\sim$1 cm^2/Vs) for band transport (55, 56). Still, future electronic transport and structural studies (e.g. to identify the precise molecular makeup of the nanofibers) are needed to resolve the underlying mechanism, particularly if conduction operates in a more complex regime than band theory or hopping, where electron transport may be delocalized transiently or permanently over several sites along the nanofibers (57, 58).

Conclusion

In summary, this study presents a detailed electronic characterization of *Candidatus* Electronema cable bacteria from Southern California freshwater sediments. The cell

envelope characteristics of the freshwater cable bacteria, including the characteristic periplasmic nanofiber network, are consistent with previous observations of the globally distributed cable bacteria. Conductive atomic force and electrostatic force microscopies confirmed the role of the nanofiber network as the conductive conduit of freshwater cable bacteria, as previously observed in marine cable bacteria. In addition, current-voltage measurements confirmed the conductivity of whole cable bacterial filaments, while hinting that the conductivity of the freshwater filaments may be less sensitive to oxygen exposure than previously observed. The conductivity of the periplasmic nanofibers from four-probe electronic transport measurements was estimated at 0.1 S/cm, a value high enough to support the electron current densities linking sulfide oxidation to oxygen reduction through the electric metabolism of cable bacteria in sediment environments. While electronic characterization of this long-distance electron transport previously focused on marine cables, our measurements shed light on the conductivity of freshwater cable bacteria, and highlight the potential applications of cable bacteria as bioelectronic conduits with both environmental and future biotechnological relevance.

Acknowledgments

This work was supported by supported by the W.M. Keck Foundation award 8626 and Gordon and Betty Moore Foundation grant 10148. We thank Dr. Edith Read and the Friends of Ballona Wetlands organization for their kind help and sampling permission. We would like to thank the Nano3 cleanroom at the University of California, San Diego for microfabrication services. TEM imaging was performed at the Core Center of Excellence in Nano Imaging at the University of Southern California.

References

1. Gray HB & Winkler JR (2003) Electron tunneling through proteins. *Quarterly Reviews of Biophysics* 36(3):341-372.
2. Atkinson JT, Chavez MS, Niman CM, & El-Naggar MY (2023) Living electronics: A catalogue of engineered living electronic components. *Microbial Biotechnology* 16(3):507-533.
3. Wang FB, *et al.* (2019) Structure of Microbial Nanowires Reveals Stacked Hemes that Transport Electrons over Micrometers. *Cell* 177(2):361-+.
4. Wang FB, *et al.* (2022) Structure of Geobacter OmcZ filaments suggests extracellular cytochrome polymers evolved independently multiple times. *Elife* 11.
5. Yates MD, *et al.* (2016) Measuring conductivity of living Geobacter sulfurreducens biofilms. *Nature Nanotechnology* 11(11):910-913.
6. Xu S, Barrozo A, Tender LM, Krylov AI, & El-Naggar MY (2018) Multiheme Cytochrome Mediated Redox Conduction through Shewanella oneidensis MR-1 Cells. *Journal of the American Chemical Society* 140(32):10085-10089.
7. McGlynn SE, Chadwick GL, Kempes CP, & Orphan VJ (2015) Single cell activity reveals direct electron transfer in methanotrophic consortia. *Nature* 526(7574):531-535.
8. Pfeffer C, *et al.* (2012) Filamentous bacteria transport electrons over centimetre distances. *Nature* 491(7423):218-221.
9. Nielsen LP, Risgaard-Petersen N, Fossing H, Christensen PB, & Sayama M (2010) Electric currents couple spatially separated biogeochemical processes in marine sediment. *Nature* 463(7284):1071-1074.
10. Meysman FJR, Risgaard-Petersen N, Malkin SY, & Nielsen LP (2015) The geochemical fingerprint of microbial long-distance electron transport in the seafloor. *Geochim Cosmochim Ac* 152:122-142.
11. Risgaard-Petersen N, *et al.* (2015) Cable Bacteria in Freshwater Sediments. *Appl Environ Microbiol* 81(17):6003-6011.
12. Marzocchi U, *et al.* (2018) Transient bottom water oxygenation creates a niche for cable bacteria in long-term anoxic sediments of the Eastern Gotland Basin. *Environmental microbiology* 20(8):3031-3041.
13. Schauer R, *et al.* (2014) Succession of cable bacteria and electric currents in marine sediment. *ISME J* 8(6):1314-1322.
14. Malkin SY, *et al.* (2014) Natural occurrence of microbial sulphur oxidation by long-range electron transport in the seafloor. *ISME J* 8(9):1843-1854.
15. Burdorf LDW, Hidalgo-Martinez S, Cook PLM, & Meysman FJR (2016) Long-distance electron transport by cable bacteria in mangrove sediments. *Mar Ecol Prog Ser* 545:1-8.
16. van de Velde S, *et al.* (2016) The impact of electrogenic sulfur oxidation on the biogeochemistry of coastal sediments: A field study. *Geochim Cosmochim Ac* 194:211-232.
17. Muller H, Marozava S, Probst AJ, & Meckenstock RU (2020) Groundwater cable bacteria conserve energy by sulfur disproportionation. *ISME J* 14(2):623-634.
18. Kjeldsen KU, *et al.* (2019) On the evolution and physiology of cable bacteria. *Proc Natl Acad Sci U S A* 116(38):19116-19125.
19. Marzocchi U, *et al.* (2014) Electric coupling between distant nitrate reduction and sulfide oxidation in marine sediment. *ISME J* 8(8):1682-1690.
20. Cornelissen R, *et al.* (2018) The Cell Envelope Structure of Cable Bacteria. *Frontiers in microbiology* 9.
21. Leonid D, *et al.* (2023) Comparative electric and ultrastructural studies of cable bacteria reveal new components of conduction machinery. *bioRxiv*:2023.2005.2024.541955.

22. Meysman FJR, *et al.* (2019) A highly conductive fibre network enables centimetre-scale electron transport in multicellular cable bacteria. *Nature communications* 10(1):4120.
23. Thiruvallur Eachambadi R, *et al.* (2020) An Ordered and Fail-Safe Electrical Network in Cable Bacteria. *Advanced biosystems* 4(7):e2000006.
24. Bonne R, *et al.* (2020) Intrinsic electrical properties of cable bacteria reveal an Arrhenius temperature dependence. *Sci Rep-Uk* 10(1).
25. Boschker HTS, *et al.* (2021) Efficient long-range conduction in cable bacteria through nickel protein wires. *Nature communications* 12(1).
26. Trojan D, *et al.* (2016) A taxonomic framework for cable bacteria and proposal of the candidate genera Electrothrix and Electronema. *Systematic and applied microbiology* 39(5):297-306.
27. Muller H, *et al.* (2016) Long-distance electron transfer by cable bacteria in aquifer sediments. *ISME J* 10(8):2010-2019.
28. Sandfeld T, Marzocchi U, Petro C, Schramm A, & Risgaard-Petersen N (2020) Electrogenic sulfide oxidation mediated by cable bacteria stimulates sulfate reduction in freshwater sediments. *ISME J* 14(5):1233-1246.
29. Scholz VV, Meckenstock RU, Nielsen LP, & Risgaard-Petersen N (2020) Cable bacteria reduce methane emissions from rice-vegetated soils. *Nature communications* 11(1):1878.
30. Risgaard-Petersen N, Damgaard LR, Revil A, & Nielsen LP (2014) Mapping electron sources and sinks in a marine biogeobattery. *Journal of Geophysical Research-Biogeosciences* 119(8):1475-1486.
31. Environmental-Protection-Agency US (2012) Los Angeles Area Lakes Total Maximum Daily Loads-- Section 4 Peck Road Park Lake https://19january2017snapshot.epa.gov/www2013/region2019/water/tmdl/la-lakes/LALakesTMDLsSection2014PeckRoadParkLake.pdf.
32. Kjeldsen KU, *et al.* (2007) Diversity of sulfate-reducing bacteria from an extreme hypersaline sediment, Great Salt Lake (Utah). *FEMS microbiology ecology* 60(2):287-298.
33. Ludwig W, *et al.* (2004) ARB: a software environment for sequence data. *Nucleic Acids Res* 32(4):1363-1371.
34. Quast C, *et al.* (2013) The SILVA ribosomal RNA gene database project: improved data processing and web-based tools. *Nucleic Acids Res* 41(D1):D590-D596.
35. Sass H, Wieringa E, Cypionka H, Babenzien HD, & Overmann J (1998) High genetic and physiological diversity of sulfate-reducing bacteria isolated from an oligotrophic lake sediment. *Arch Microbiol* 170(4):243-251.
36. Ferrer M, *et al.* (2011) Taxonomic and Functional Metagenomic Profiling of the Microbial Community in the Anoxic Sediment of a Sub-saline Shallow Lake (Laguna de Carrizo, Central Spain). *Microbial Ecology* 62(4):824-837.
37. Junghare M & Schink B (2015) Desulfoprunum benzoelyticum gen. nov., sp. nov., a Gram-stain-negative, benzoate-degrading, sulfate-reducing bacterium isolated from a wastewater treatment plant. *International journal of systematic and evolutionary microbiology* 65(Pt 1):77-84.
38. Martin F, *et al.* (2012) Betaproteobacteria dominance and diversity shifts in the bacterial community of a PAH-contaminated soil exposed to phenanthrene. *Environmental pollution* 162:345-353.
39. Dorador C, Vila I, Witzel KP, & Imhoff JF (2013) Bacterial and archaeal diversity in high altitude wetlands of the Chilean Altiplano. *Fund Appl Limnol* 182(2):135-159.
40. Tonolla M, Demarta A, Peduzzi S, Hahn D, & Peduzzi R (2000) In situ analysis of sulfate-reducing bacteria related to Desulfocapsa thiozymogenes in the chemocline of meromictic Lake Cadagno (Switzerland). *Appl Environ Microb* 66(2):820-824.

41. Dorador C, Castillo G, Witzel KP, & Vila I (2007) Bacterial diversity in the sediments of a temperate artificial lake, Rapel reservoir. *Rev Chil Hist Nat* 80(2):213-224.
42. Ali M, Shaw DR, Albertsen M, & Saikaly PE (2020) Comparative Genome-Centric Analysis of Freshwater and Marine ANAMMOX Cultures Suggests Functional Redundancy in Nitrogen Removal Processes. *Frontiers in microbiology* 11.
43. Sait M, Hugenholtz P, & Janssen PH (2002) Cultivation of globally distributed soil bacteria from phylogenetic lineages previously only detected in cultivation-independent surveys. *Environmental microbiology* 4(11):654-666.
44. Momper L, Aronson HS, & Amend JP (2018) Genomic Description of 'Candidatus Abyssubacteria,' a Novel Subsurface Lineage Within the Candidate Phylum Hydrogenedentes. *Frontiers in microbiology* 9.
45. Burdorf LDW, *et al.* (2017) Long-distance electron transport occurs globally in marine sediments. *Biogeosciences* 14(3):683-701.
46. Thorup C, *et al.* (2021) How to grow your cable bacteria: Establishment of a stable single-strain culture in sediment and proposal of Candidatus Electronema aureum GS. *Systematic and Applied Microbiology* 44(5).
47. Scholz VV, *et al.* (2021) Cable bacteria at oxygen-releasing roots of aquatic plants: a widespread and diverse plant-microbe association. *New Phytologist* 232(5):2138-2151.
48. Staii C, Johnson AT, & Pinto NJ (2004) Quantitative analysis of scanning conductance microscopy. *Nano Letters* 4(5):859-862.
49. Risgaard-Petersen N, Revil A, Meister P, & Nielsen LP (2012) Sulfur, iron-, and calcium cycling associated with natural electric currents running through marine sediment. *Geochim Cosmochim Ac* 92:1-13.
50. Larsen S, Nielsen LP, & Schramm A (2015) Cable bacteria associated with long-distance electron transport in New England salt marsh sediment. *Environ Microbiol Rep* 7(2):175-179.
51. Seitaj D, *et al.* (2015) Cable bacteria generate a firewall against euxinia in seasonally hypoxic basins. *P Natl Acad Sci USA* 112(43):13278-13283.
52. Sulu-Gambari F, *et al.* (2016) Cable Bacteria Control Iron-Phosphorus Dynamics in Sediments of a Coastal Hypoxic Basin. *Environ Sci Technol* 50(3):1227-1233.
53. Geelhoed JS, van de Velde SJ, & Meysman FJR (2020) Quantification of Cable Bacteria in Marine Sediments via qPCR. *Frontiers in Microbiology* 11.
54. van de Velde S, Callebaut I, Gao Y, & Meysman FJR (2017) Impact of electrogenic sulfur oxidation on trace metal cycling in a coastal sediment. *Chemical Geology* 452:9-23.
55. Polizzi NF, Skourtis SS, & Beratan DN (2012) Physical constraints on charge transport through bacterial nanowires. *Faraday Discussions* 155:43-62.
56. Pirbadian S & El-Naggar MY (2012) Multistep hopping and extracellular charge transfer in microbial redox chains. *Physical Chemistry Chemical Physics* 14:13802-13808.
57. Beratan DN (2019) Why Are DNA and Protein Electron Transfer So Different? *Annual Review of Physical Chemistry, Vol 70* 70:71-97.
58. Beratan DN, *et al.* (2015) Charge Transfer in Dynamical Biosystems, or The Treachery of (Static) Images. *Accounts of Chemical Research* 48(2):474-481.

Figures and Tables

Figure 1. (A) Sampling sites for cable bacteria from the Ballona Freshwater Marsh and Mungi Lake, California, USA. **(B)** Enrichment in laboratory incubations resulted in a high density of long cable bacteria filaments, some of which could be observed directly in cracked sediments. Scale bar: 35 mm. **(C)** Optical microscopy revealed the characteristic end-to-end multicellular morphology of the cable bacteria filaments, revealing occasional darker cells (black arrows) with slightly larger diameters, consistent with 'empty cage' cells scaffolded by the nanofiber network of cable bacteria (see Figure 2). Scale bar: 5 µm.

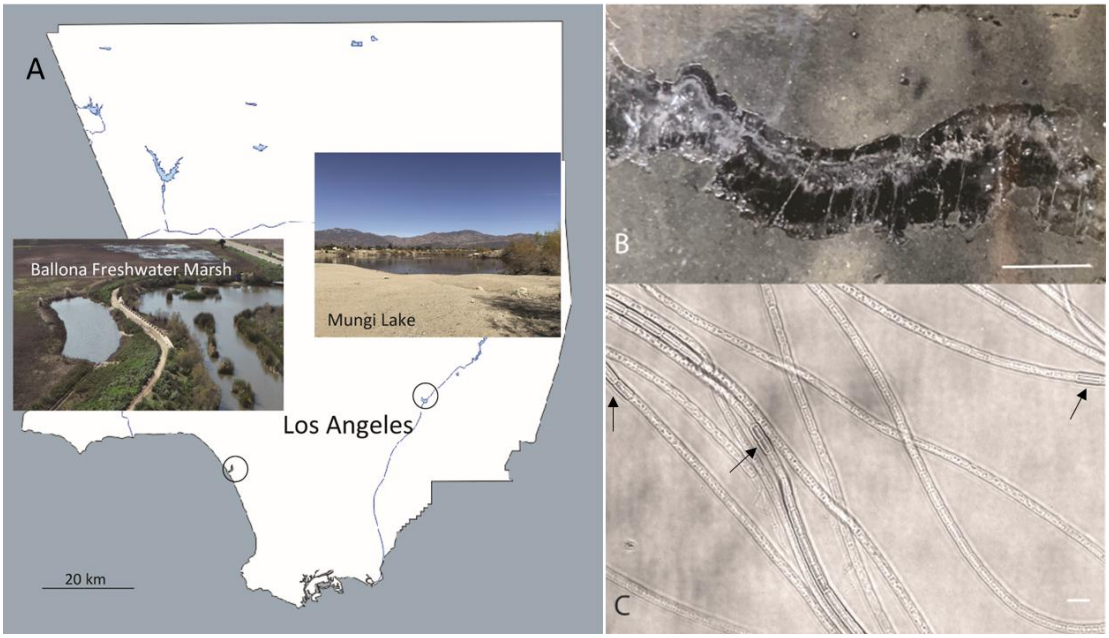

Figure 2. (A) Transmission electron microscopy of Ballona Freshwater Marsh cable bacteria showing the characteristic cell surface ridge pattern. Scale bar: 1 µm. (B) The underlying network of parallel periplasmic nanofibers can be seen clearly in occasional degraded cells as the electron-dense scaffold of "empty cages". Small intracellular dark globules (white arrows) are consistent with polyphosphate granules commonly found in marine cable filaments. Scale bar: 2.5 µm.

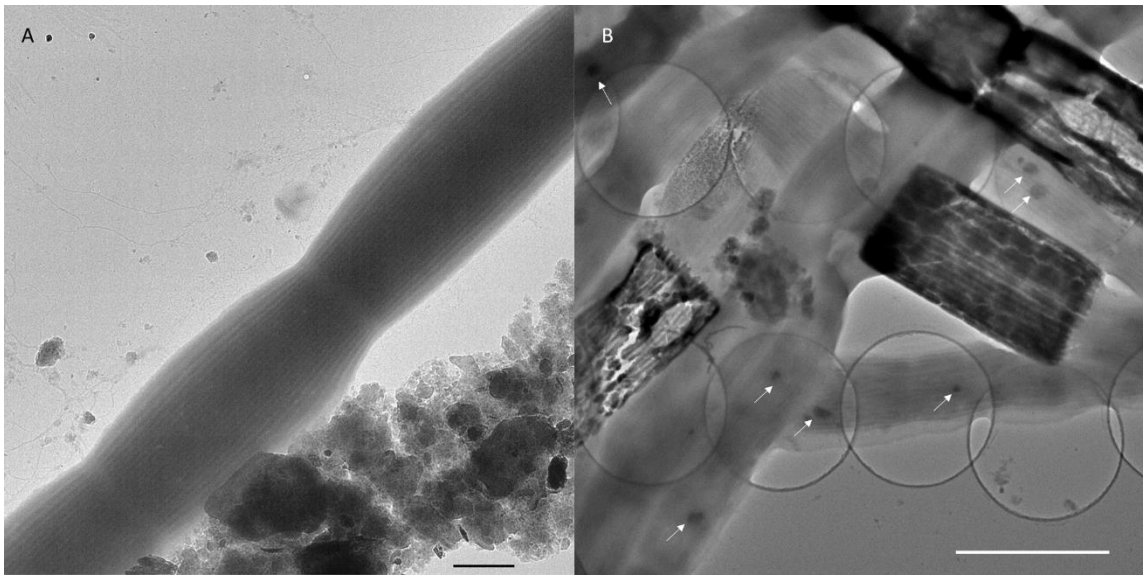

Figure 3. Phylogenetic tree based on 16S rRNA gene sequences of the Ballona Freshwater Marsh and Mungi Lake cable bacteria, other cable bacterial Candidatus taxa, and representatives of isolated members from the family *Desulfobulbaceae*. Scale bar represents 10% estimated sequence divergence. Bootstrap numbers (1000 re-samplings) > 70 are listed.

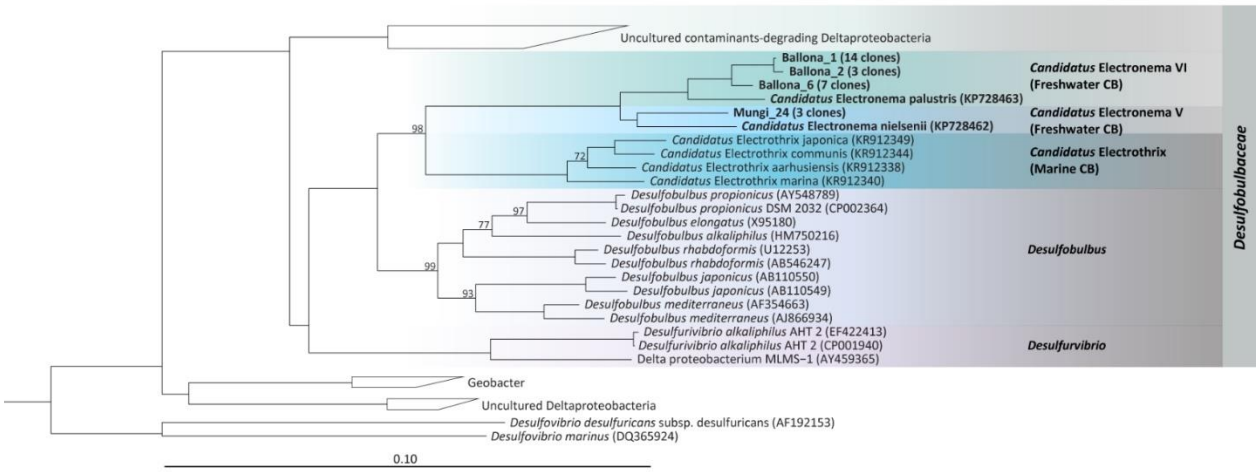

Figure 4. (A) Tapping mode atomic force microscopy of freshwater cable bacteria near the junction between two cells. Inset is a cross-sectional line scan showing cell surface ridge pattern. **(B)** Atomic force phase image corresponding to the topographical scan and showing the ridge pattern in high contrast. **(C)** Electrostatic force microscopy image with a 6 V tip bias, collected from the retrace scan at 50 nm fixed height above the cable surface. The contrast in this image stems from the electric force rather than topography. **(D)** The voltage dependence of the electrostatic interaction (phase shift, $\Delta\phi$, of the ridges with higher electric force relative to inter-ridge regions) between the conductive tip and the same cable bacterial filament from (C).

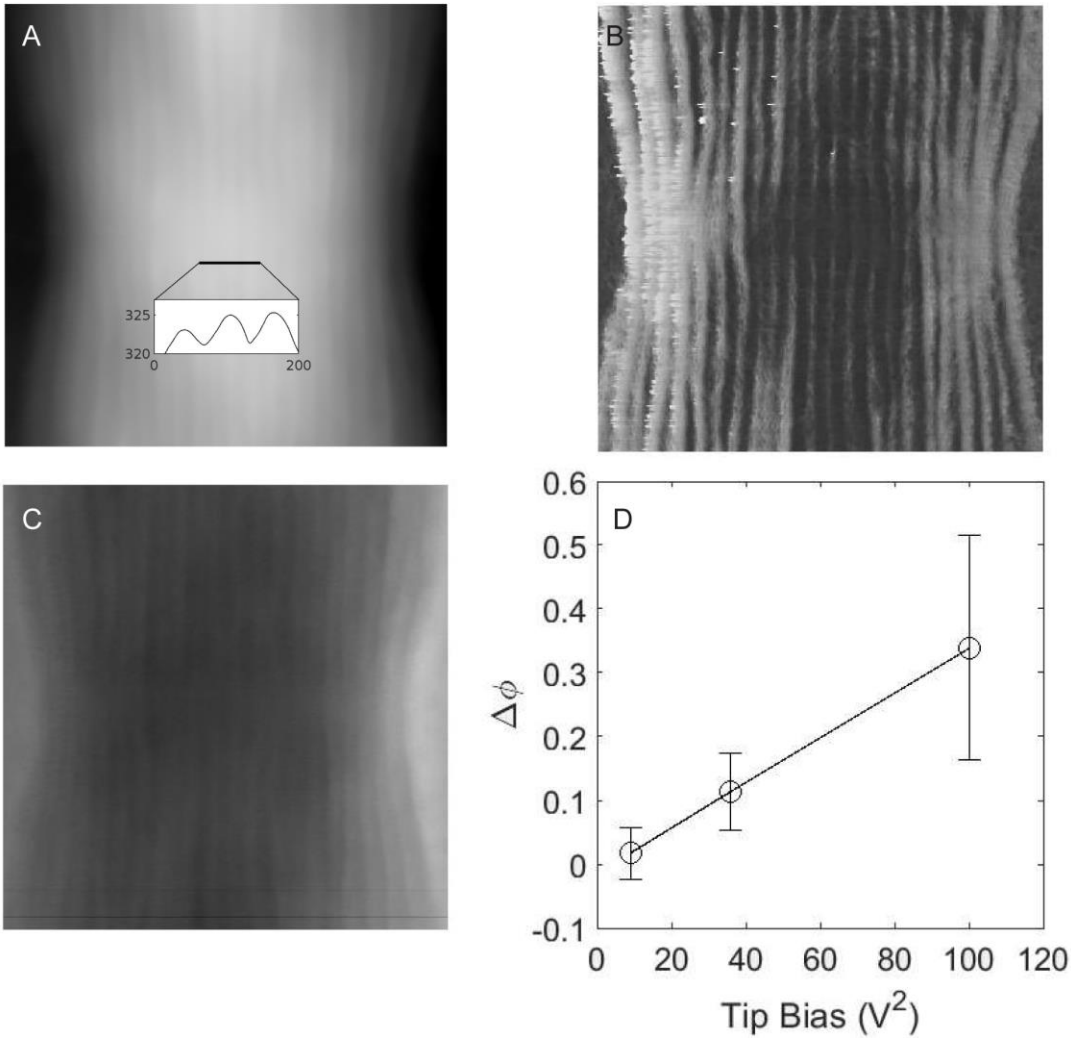

Figure 5. Current-voltage (I-V) measurements of Ballona Freshwater Marsh cable bacteria on gold interdigitated array (IDA) microelectrodes (3 µm gap between the fingers of the two electrode bands). For this measurement, two cable filaments were deposited on the IDA (inset). The I-V measurements (black) show a modest increase in conductance over time (3 hours) during consecutive measurements in an air-free environment (95% N_2 and 5% H_2). Upon air exposure (red) the conductance slowly declined over time (2.7 hours), and conductance recovered partially after re-insertion into an air-free environment (green). Arrow direction denotes measurements over time for a particular condition.

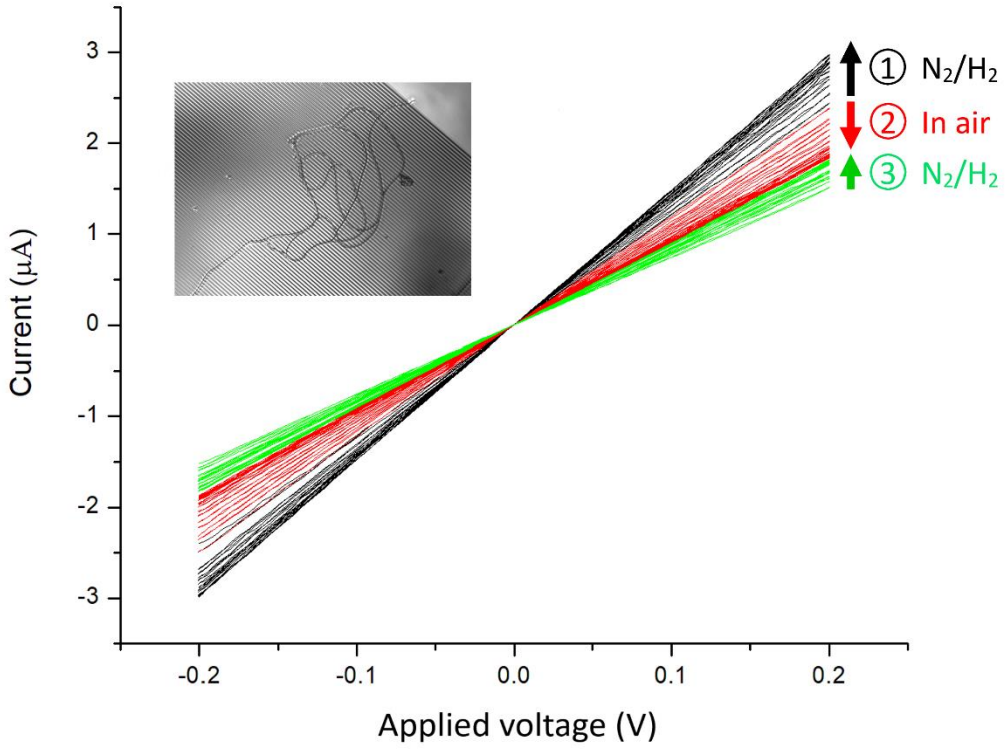

Figure 6. Representative atomic force microscopy amplitude images of Ballona freshwater cable bacteria filaments spanning the insulating quartz gap between yellow false colored gold **(A and B)** and indium tin oxide **(C)** microelectrodes. Colored crosses mark the conductive tip location in each sample where point current-voltage (I-V) spectra were collected to measure electron transport between the microelectrodes and tip. Scale bars: 2.5 μm. **(D)** I-V responses from the three representative cables. Line color corresponds to the color of the corresponding cross mark in (A-C).

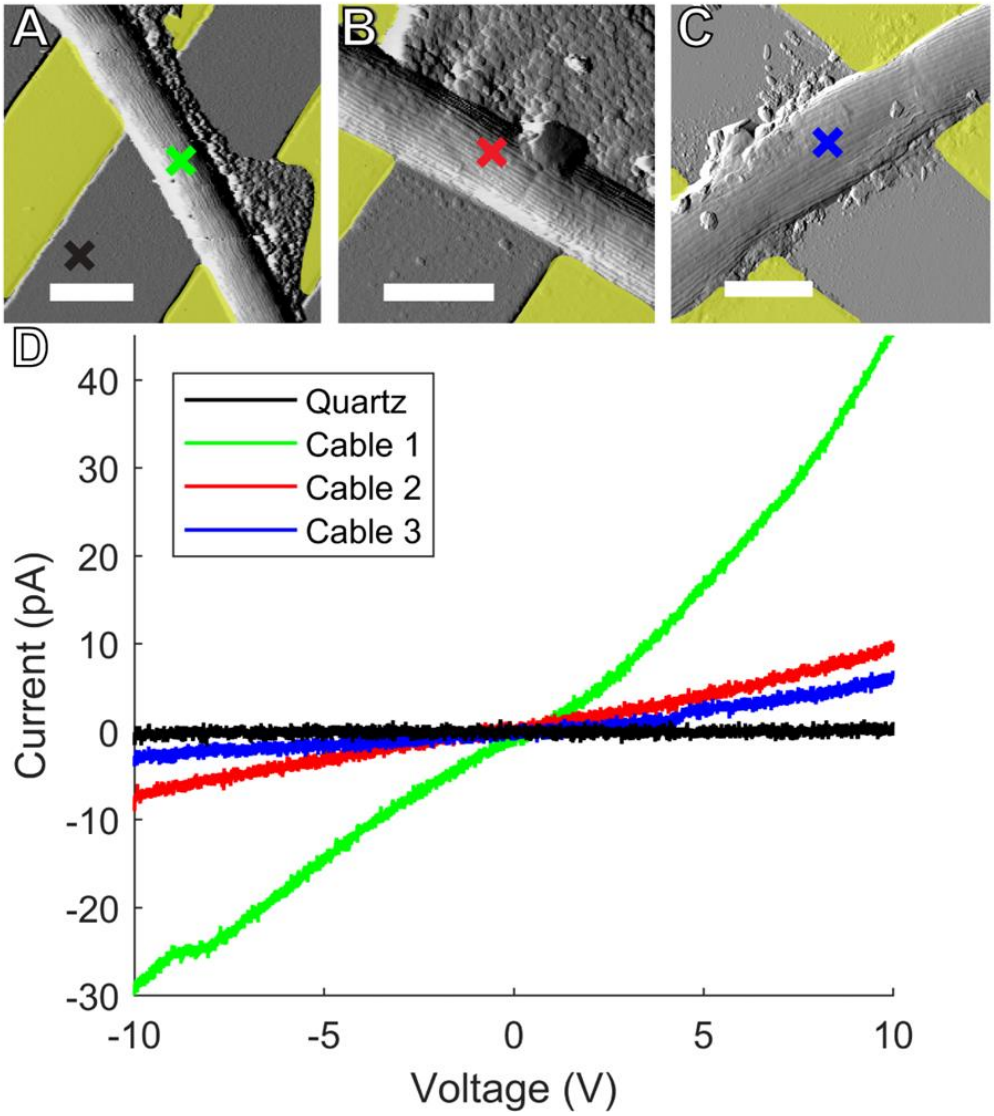

Figure 7. (A) A spatial montage of three consecutive tapping atomic force microscopy amplitude images of two parallel Mungi Lake freshwater cable bacteria in contact with, and extending away from, an electrode (false colored yellow). Scale bar: 3 μm. **(B)** Conductive atomic force current map images of the same sections shown in (A) with 5 V bias between the underlying electrode and conductive tip. The observed current signals largely correlate with the corresponding cell surface ridge pattern in (A).

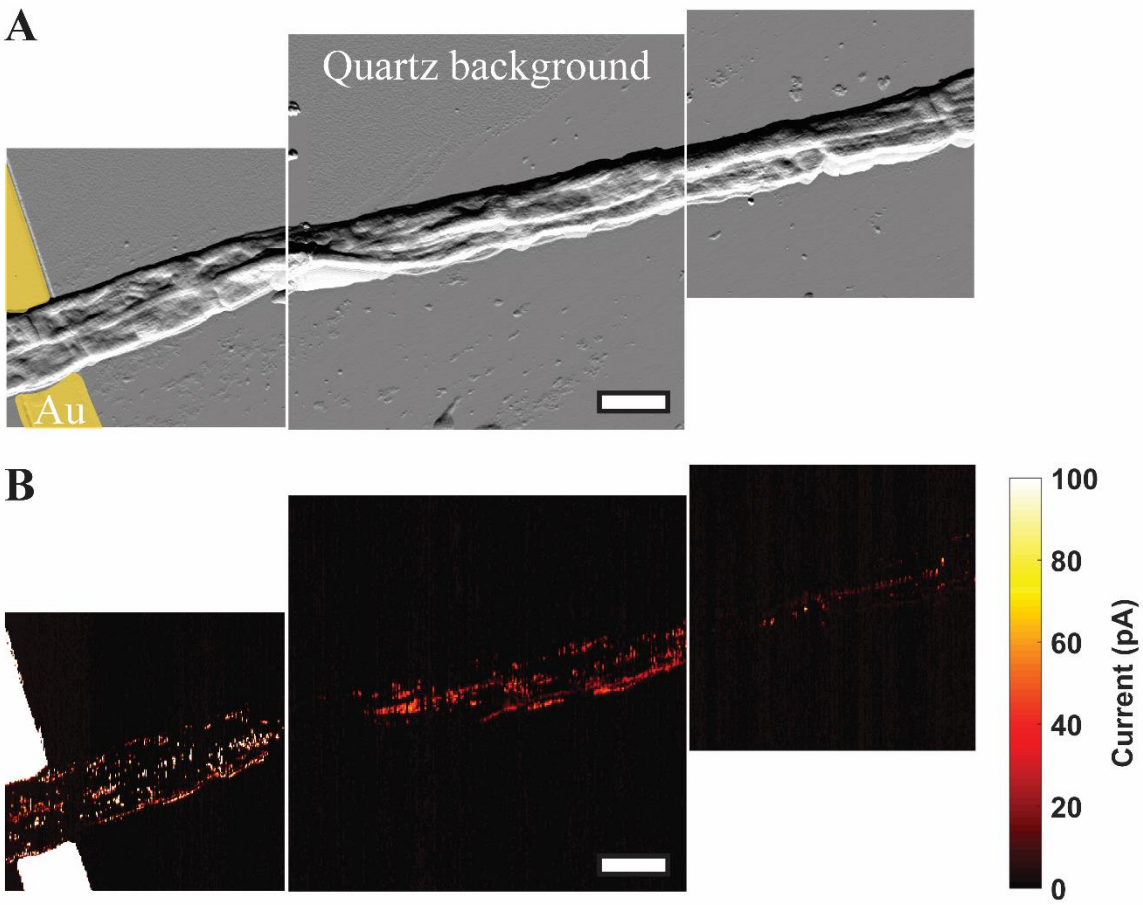

Figure 8. Four-probe current-voltage measurements of Mungi Lake freshwater cable bacteria filaments, shown for two different separations between the two inner probes. Inset: representative image of cable bacteria filaments across a four-probe device. Each data point is the average of three data points, and the error bars represent the standard deviation.

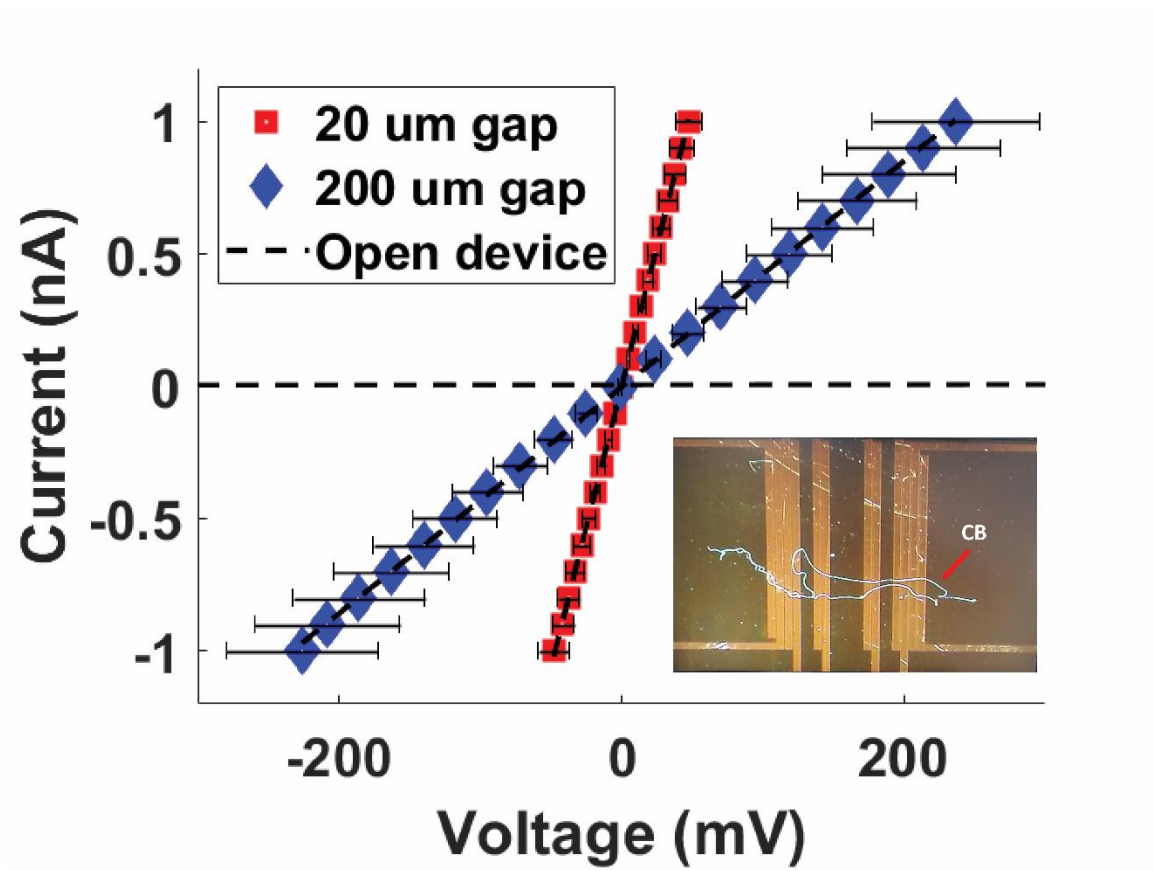

Figure S1. An example of sensitivity of conduction in cable bacteria to air exposure. Consistent current is monitored overnight for a Ballona freshwater sediment cable bacteria filament on an IDA under N_2 flow conditions, with an 800 mV difference between the two microelectrode bands. The current immediately declined upon interruption of N_2 flow and exposure to air.

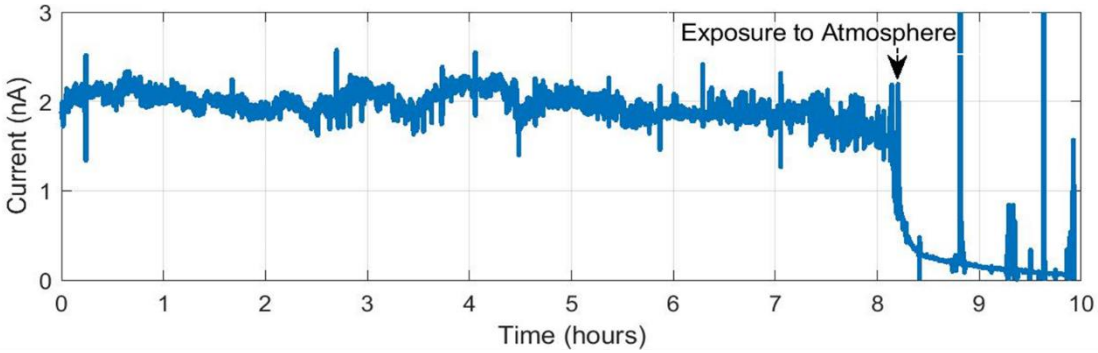

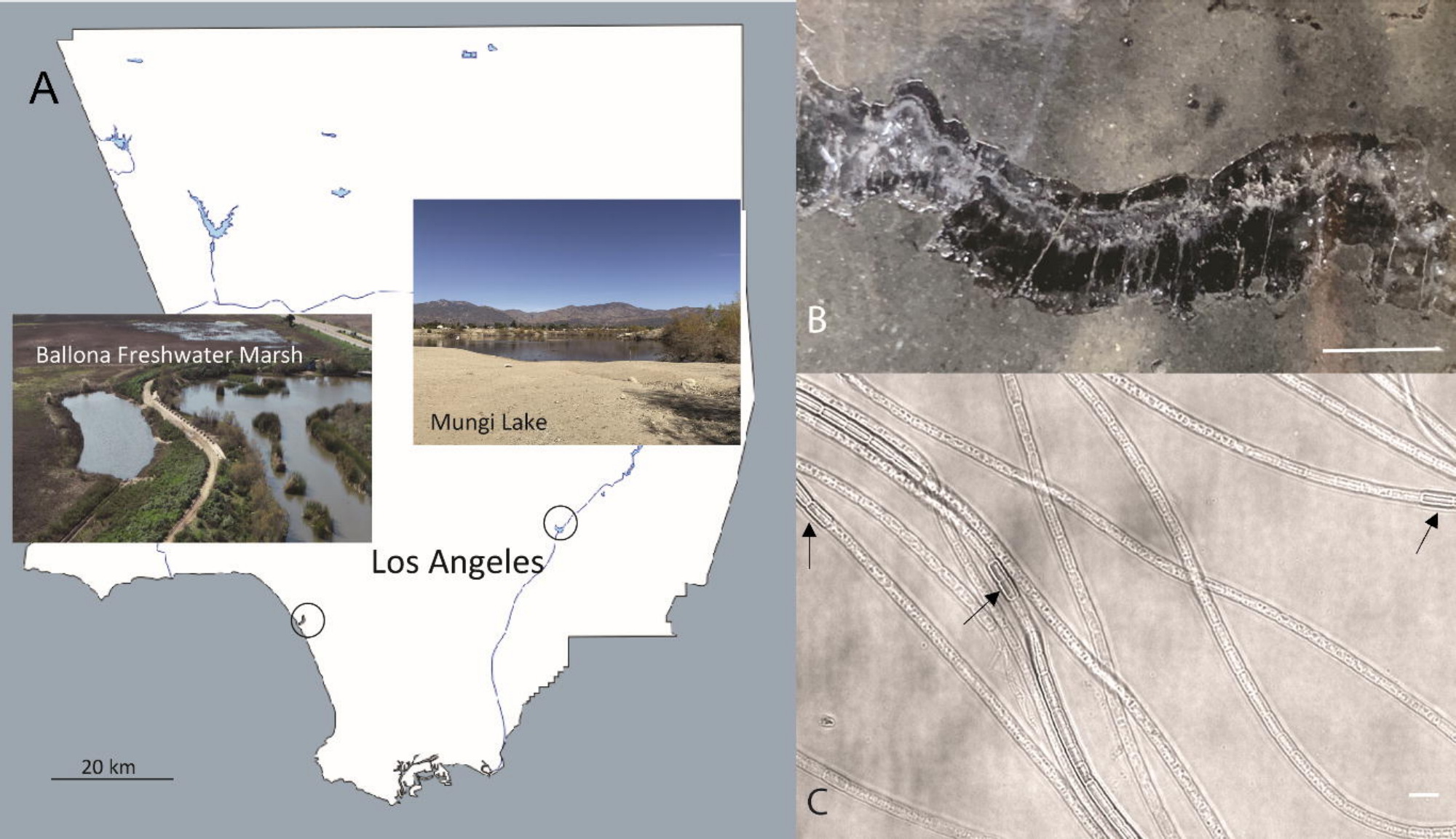
A
Ballona Freshwater Marsh
Mungi Lake
Los Angeles
20 km
B
C

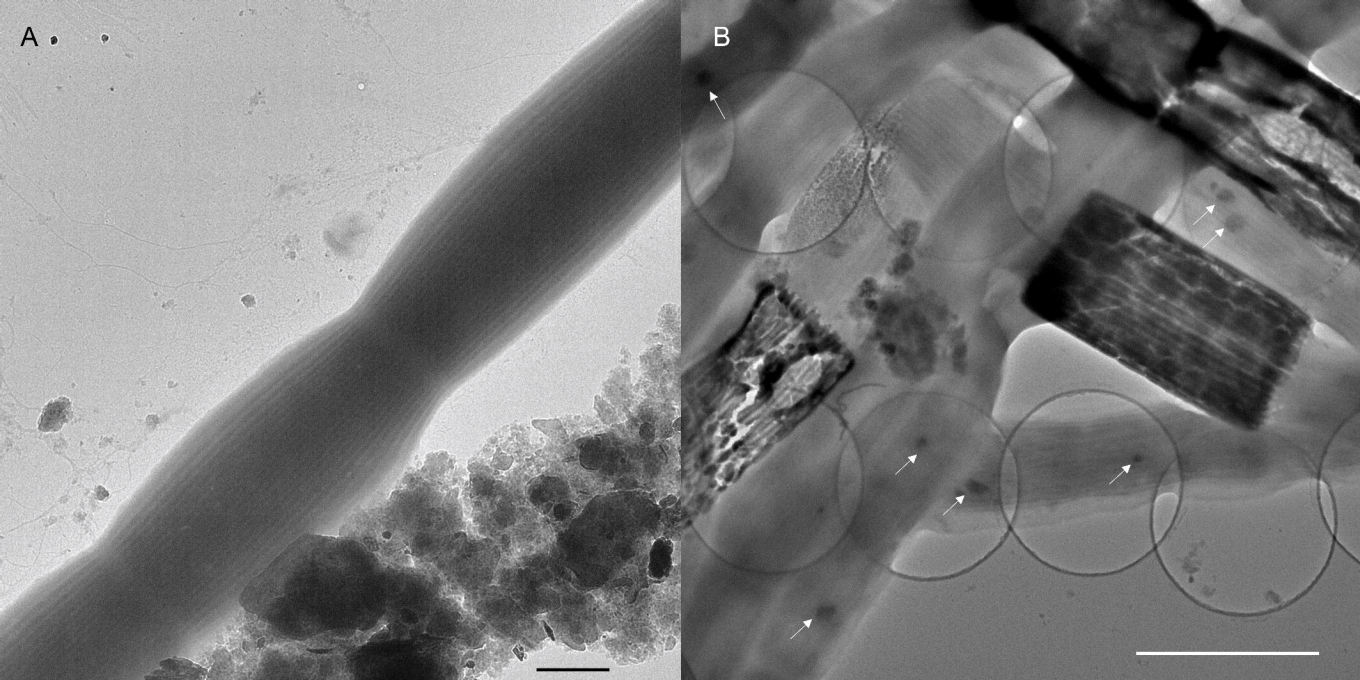
A
B

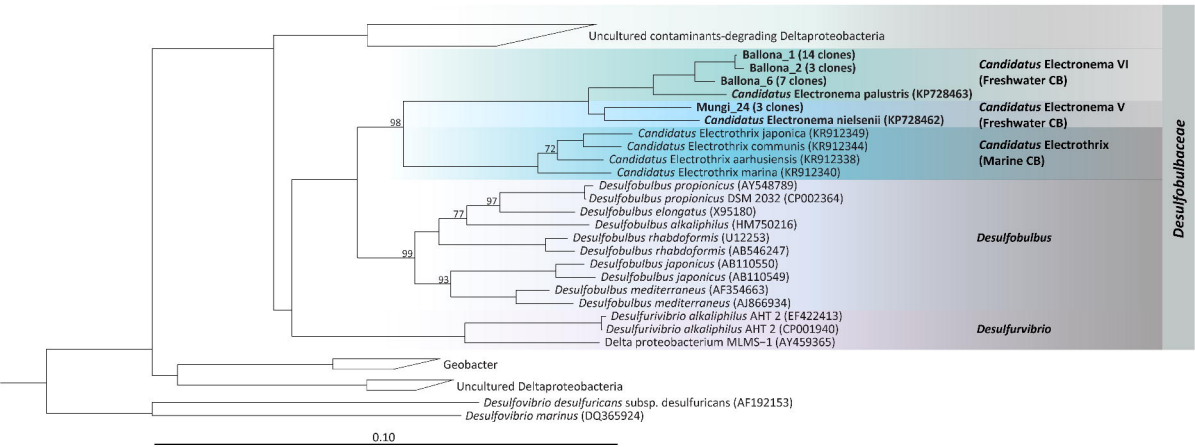
Uncultured contaminants-degrading Deltaproteobacteria
Ballona_1 (14 clones)
Ballona_2 (3 clones)
Ballona_6 (7 clones)
Candidatus Electronema palustris (KP728463)
Candidatus Electronema VI (Freshwater CB)
Mungi_24 (3 clones)
Candidatus Electronema nielsenii (KP728462)
Candidatus Electronema V (Freshwater CB)
Candidatus Electrothrix japonica (KR912349)
Candidatus Electrothrix communis (KR912344)
Candidatus Electrothrix aarhusiensis (KR912338)
Candidatus Electrothrix marina (KR912340)
Candidatus Electrothrix (Marine CB)
Desulfobulbus propionicus (AY548789)
Desulfobulbus propionicus DSM 2032 (CP002364)
Desulfobulbus elongatus (X95180)
Desulfobulbus alkaliphilus (HM750216)
Desulfobulbus rhabdoformis (U12253)
Desulfobulbus rhabdoformis (AB546247)
Desulfobulbus japonicus (AB110550)
Desulfobulbus japonicus (AB110549)
Desulfobulbus mediterraneus (AF354663)
Desulfobulbus mediterraneus (AJ866934)
Desulfobulbus
Desulfurivibrio alkaliphilus AHT 2 (EF422413)
Desulfurivibrio alkaliphilus AHT 2 (CP001940)
Delta proteobacterium MLMS-1 (AY459365)
Desulfurivibrio
Desulfobulbaceae
98
72
97
77
99
93
Geobacter
Uncultured Deltaproteobacteria
Desulfovibrio desulfuricans subsp. desulfuricans (AF192153)
Desulfovibrio marinus (DQ365924)
0.10

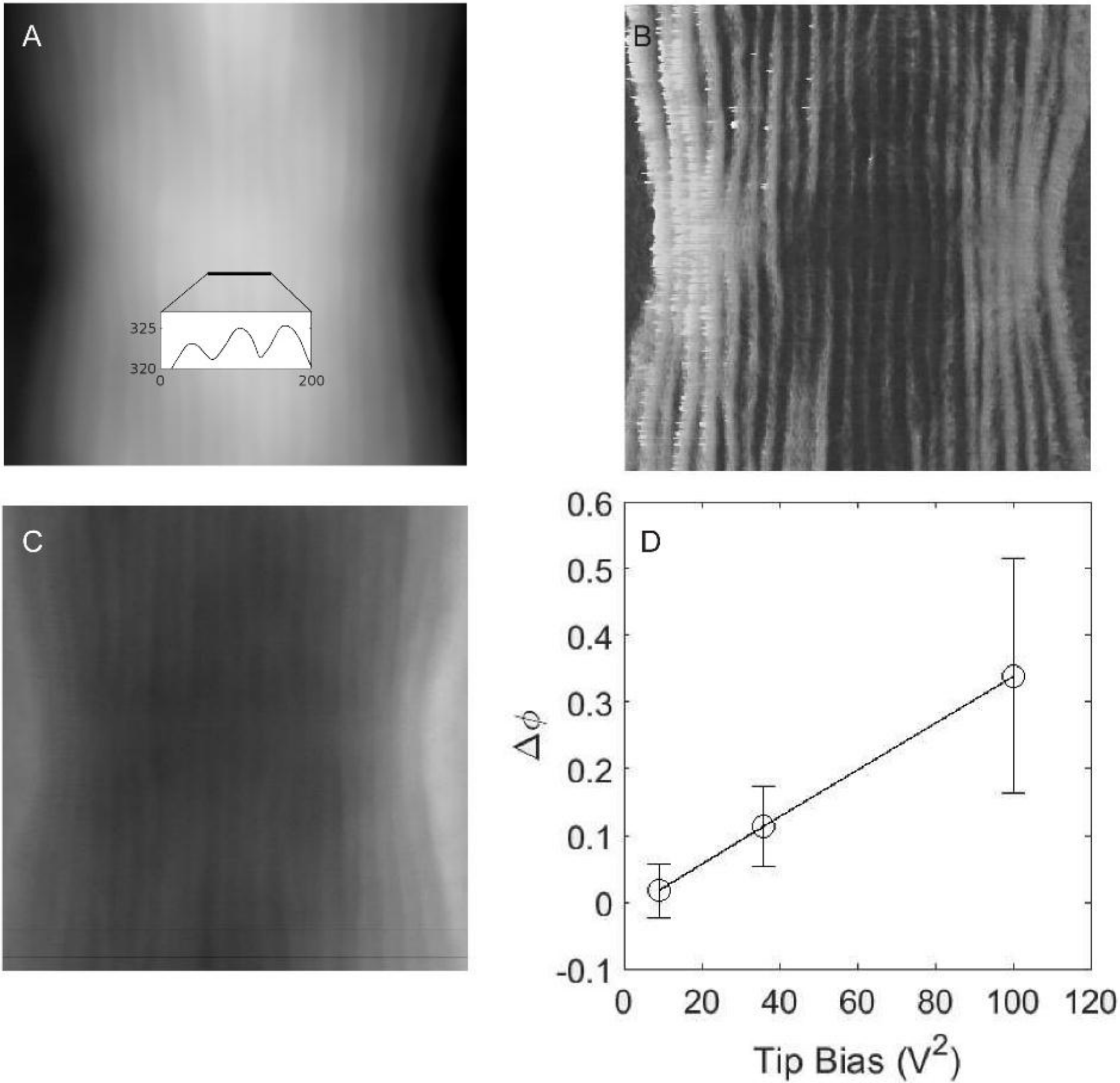
A
325
320
0
200
B
C
D
0.6
0.5
0.4
0.3
0.2
0.1
0
-0.1
$\Delta\phi$
0
20
40
60
80
100
120
Tip Bias (V^2)

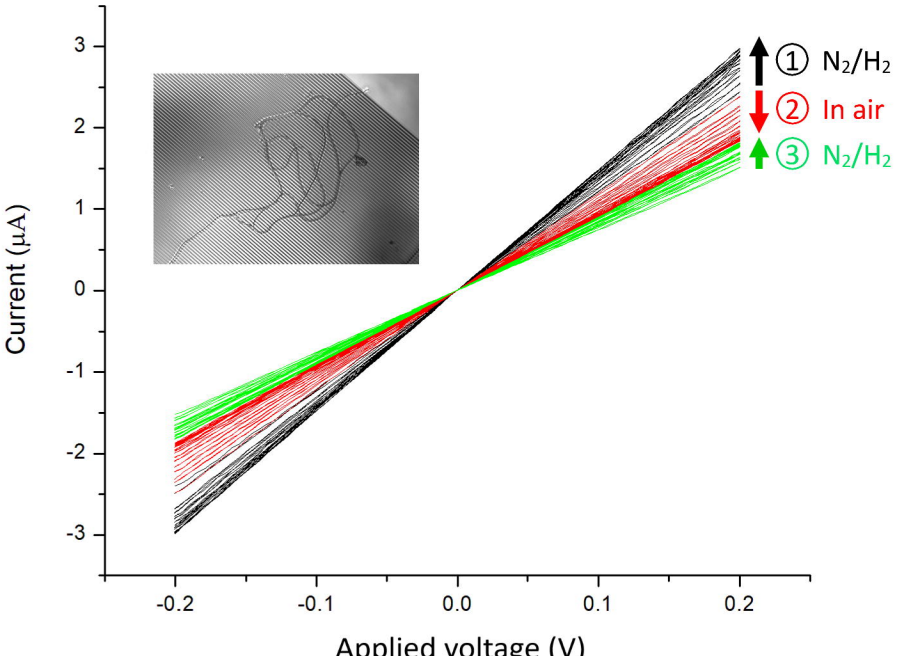
① N2/H2
② In air
③ N2/H2
Current (μA)
Applied voltage (V)
3
2
1
0
-1
-2
-3
-0.2
-0.1
0.0
0.1
0.2

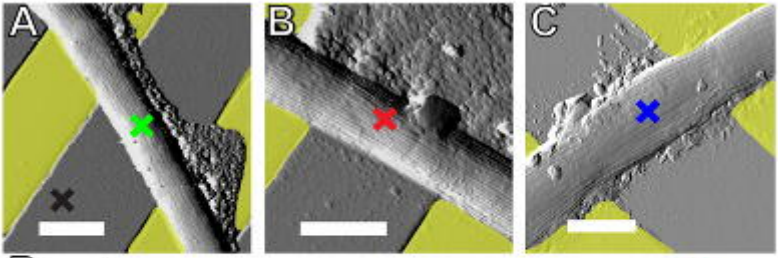
A
B
C

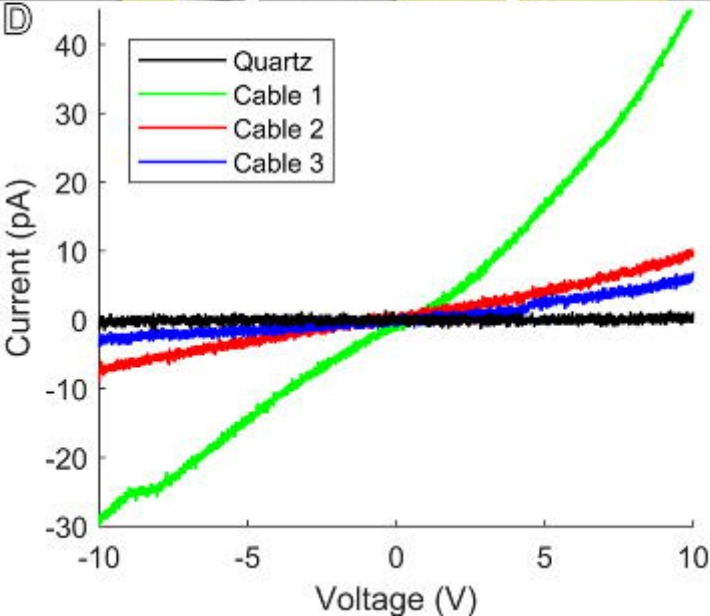
D
Quartz
Cable 1
Cable 2
Cable 3
Current (pA)
Voltage (V)
40
30
20
10
0
-10
-20
-30
-10
-5
0
5
10

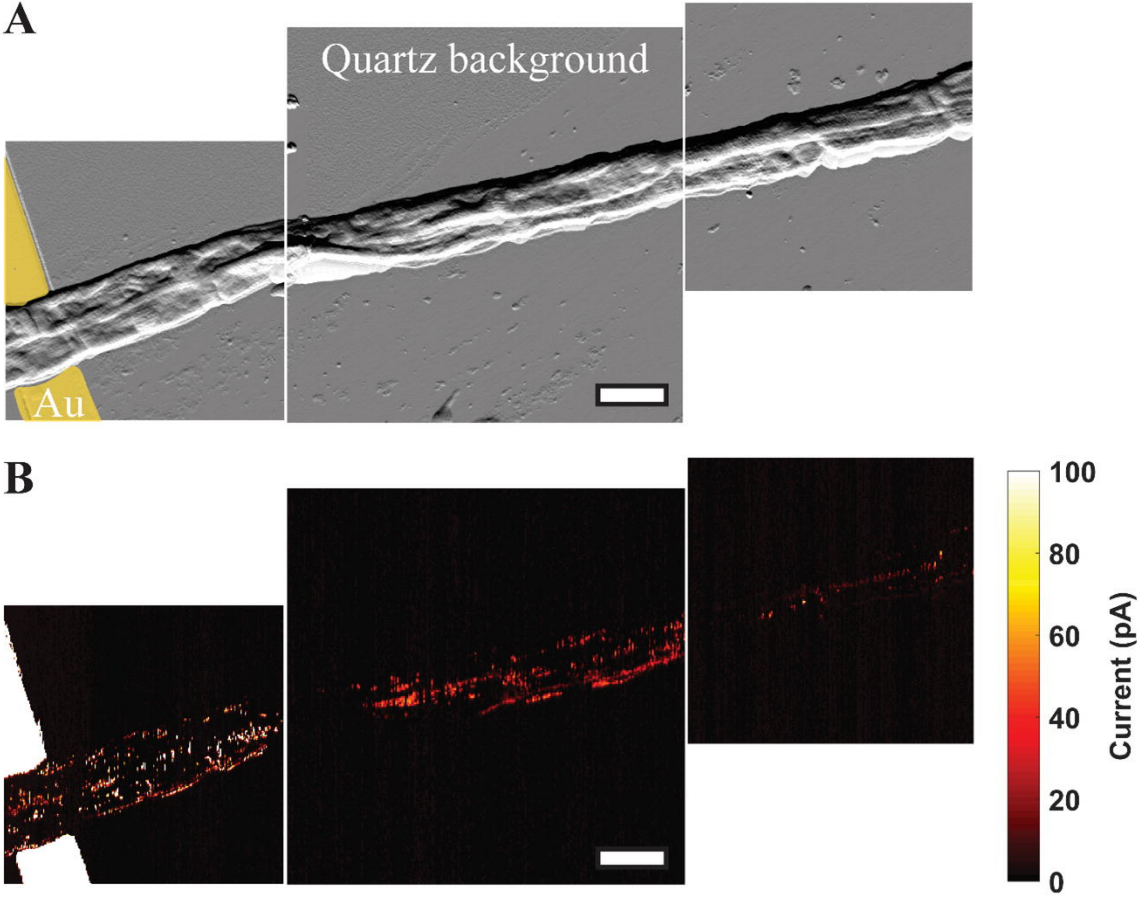
A
Quartz background
Au
B
100
80
60
40
20
0
Current (pA)

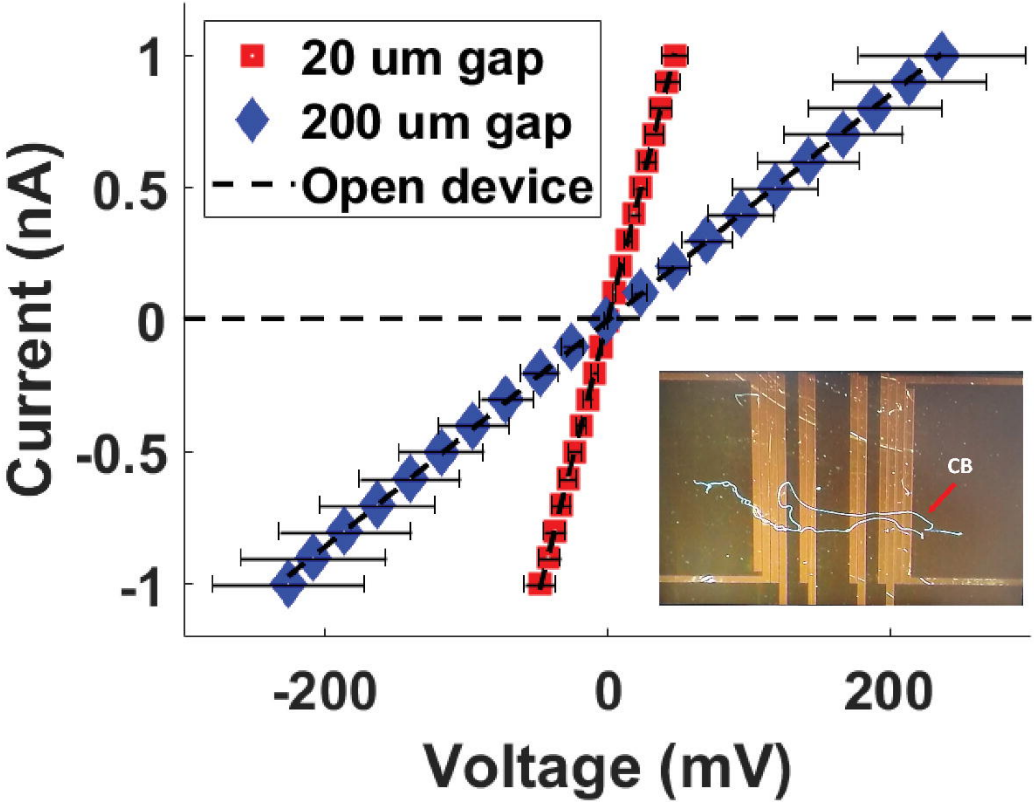
20 um gap
200 um gap
Open device
Current (nA)
Voltage (mV)
1
0.5
0
-0.5
-1
-200
0
200
CB